Construction of a three-state responsive framework from a bistable photoswitch

Jinyu Sheng[1,3], Jacopo Perego[2,3], Wojciech Danowski[1,*], Silvia Bracco[2,*], Shaoyu Chen[1], Xiaotian Zhu[1], Charl X. Bezuidenhout[2], Simon Krause[1], Wesley R. Browne,[1] Piero Sozzani[2], Angiolina Comotti[2,*], Ben L. Feringa[1,*]

1 Centre for Systems Chemistry, Stratingh Institute for Chemistry, University of Groningen, Groningen, the Netherlands.

2 Department of Materials Science, University of Milano Bicocca, Milan, Italy.

3 These authors contributed equally: Jinyu Sheng, Jacopo Perego.

e-mail: danowski@unistra.fr; silvia.bracco@unimib.it; angiolina.comotti@unimib.it; b.l.feringa@rug.nl

Abstract

The integration of photoswitchable elements into porous solids provides fascinating opportunities to modulate material responses, like molecular transport or adsorption, by external non-invasive optical stimuli. However, the synthetic strategies leading to these materials are predominately dedicated only to preserve the function of the molecular switch in the solid state while introducing new properties beyond those offered by the individual components remains challenging. Here we present a three-state switchable porous aromatic framework constructed solely from a bistable overcrowded alkene-based photoswitch. The framework was fabricated using 3D polymerization of an engineered hexadentate photoswitchable monomer by a Yamamoto coupling reaction to yield swellable and hierarchical micro-/meso-porous architectures with densely integrated photoswitches. The interplay of hierarchical porosity, flexible backbone, and reversible photoisomerization between two isomers, generates unique three distinct porosity states in the material that can be accessed in sequence upon application of external stimuli to induce sponge-like behaviour. This flexible and responsive aromatic framework represents a major step towards light-responsive materials capable to harness limited molecular-scale motion and convert it to on-demand response over hierarchical length scales towards practical output.

Bigger Picture

Incorporation of molecular photoswitches in porous solid materials offers opportunities to gain remote control of their gas uptake and release properties. These materials are designed to facilitate the isomerization in the solid by minimising the interactions between the incorporated switches and porous scaffold and consequently operate by switching between the two states inherited from the incorporated responsive moieties. Here we demonstrate a porous and flexible aromatic framework constructed exclusively from the overcrowded alkene-derived bistable molecular photoswitch. The interplay between framework flexibility, hierarchical porosity and geometrical changes associated with the

photoisomerization enabled reversible interconversion of the framework between three porosity-states orchestrated by the photoswitch. These results demonstrate that integration of molecular photoswitches in solid porous materials can lead to new functions beyond those associated with isolated molecules in solution.

Introduction

Dynamic porous materials exploit the flexibility of the individual components or the entire network to give rise to adaptive and responsive structures.[1–13] While various degrees of internal dynamics ranging from incoherent rotations[8,14,15] to geared motion[13,16] of the building blocks are ubiquitous to any structure possessing sufficient internal free volume, more complex and controllable structural deformations are required for practical applications.[17–20] Beyond this uncontrolled dynamic behaviour, the integration of light-responsive artificial molecular switches[21,22] or machines[4,5,23–28] in porous frameworks[7,29–34] allows to harness their nanoscopic motion and translate it on-demand in a non-invasive manner into the consistent and predictable change in the material performance under a wide range of external conditions. The fabrication of light-responsive porous materials allows significant advantages by alleviating the geometrical constraints associated with photoisomerization, while providing sufficient flexibility or free volume to accommodate the structural changes. Pioneering studies on azobenzenes, dithienylethenes, spiropyrans, stilbenes, and overcrowded alkenes incorporated in metal-organic (MOFs)[35–37], covalent-organic (COFs)[38–41] and porous-aromatic frameworks (PAFs)[42,43] proved the feasibility and showed opportunities offered by this approach, demonstrating modulation of a wide range of properties, such as gas-uptake, conductivity or guest-molecule separation, by isomerization of light-responsive units integrated in the framework.[44–58] In addition, several strategies circumventing the limited light-penetration depth in these materials were developed yielding systems which undergo facile photoisomerization in isolated crystals, films and even in bulk material.[30,48,51,56,59] However, photochemical isomerization in these systems is mostly restricted to the individual responsive units, which remain independent and reciprocally unaffected, thus the stimulus is not further propagated. Consequently, the functionality of the entire system and the perspectives of the materials as actuators were limited. In contrast, the insertion of active elements in each monomer unit of a 3D network allows the incorporation of multiple dynamic elements which could potentially open more accessible states or lead to the properties beyond those offered by individual elements. Therefore, we envisioned that the monomers displaying intrinsic responsiveness due to the light-driven isomerization between two distinct configurations, once polymerized, would transmit their stimulated change through the constraints to the overall network. Here we present the synthesis of a monomer functionalised with a photoswitch in its core and two lateral wings to yield a highly porous photoswitchable framework (Fig. 1a,b) collectively responsive to light and capable of switching between three distinct porosity states orchestrated by the bi-stable overcrowded alkene-derived photoswitching monomer units. The designed monomer

comprises both the overcrowded alkene photoswitch and reactive hexabromine functionalized groups which serve as responsive and porogen units (Fig. 1b). The amphifunctional structure of the monomer ensures the desired connectivity in the framework and precludes the formation of phase-separated regions or blocks of switch and porogen, producing a micro- and meso-pore architecture (state I, Fig. 1c). Indeed, we could attain the fully reversible bulk photoswitching from the stable to the metastable diastereomer, and back to the stable diastereomer using two distinct wavelengths of light, despite of high concentration of molecular switches embedded in the material. The facile back optical switching was demonstrated for the first time in porous aromatic frameworks, establishing a benchmark for the generation of a fully light-controlled photoswitchable framework (**PSF**) material. The nanoscopic isomerization process in the solid state induced by irradiation at $\lambda = 365$ nm leads to a contractile sponge-like behavior and drives the decrease of gas uptake of both mesopores and micropores (state II, Fig. 1c). Subsequently, irradiation with green light ($\lambda = 505$ nm) induces a photo-reversible expansion of the micropores (state III, Fig. 1c) whilst the mesoporous region could be entirely regenerated by swelling the framework in a solvent and subsequent activation, thus regenerating pristine material (state I, Fig. 1c). The PSF material acts as a mechanized nano-sponge switching between three distinct states arising from interactions of the bi-stable switch with the highly robust yet flexible architecture which provides sufficient free volume around the photoswitches to allow for unhindered movement in the solid-state. The present system features various aspects of novelty: i) one switch moiety between two porogenic units which ensures well-defined connectivity, topology and stoichiometry (Figure 1a, top), in contrast to framework materials with broad range of connectivities, topologies and defectiveness (Figure 1a, bottom); ii) the framework architecture is further translated in the distinctly different properties showing remarkable swelling being a basis for the fully reversible nanosponge-like behaviour; iii) in addition to the microporosity, large hysteresis in the adsorption isotherms associated with the meso-porosity, which along with the green-light responsivity of the photoswitch embedded in the framework, form the basis for the unique feature of reversible control of three distinct porous states due to the cooperativity between switch and flexible framework. These findings indicate that the nanoscopic isomerization of the photoswitch units involve not just the core, but also induce the conformational change of the lateral moieties, triggering the rearrangement of the flexible framework and leading to the control of nano-sponge properties.

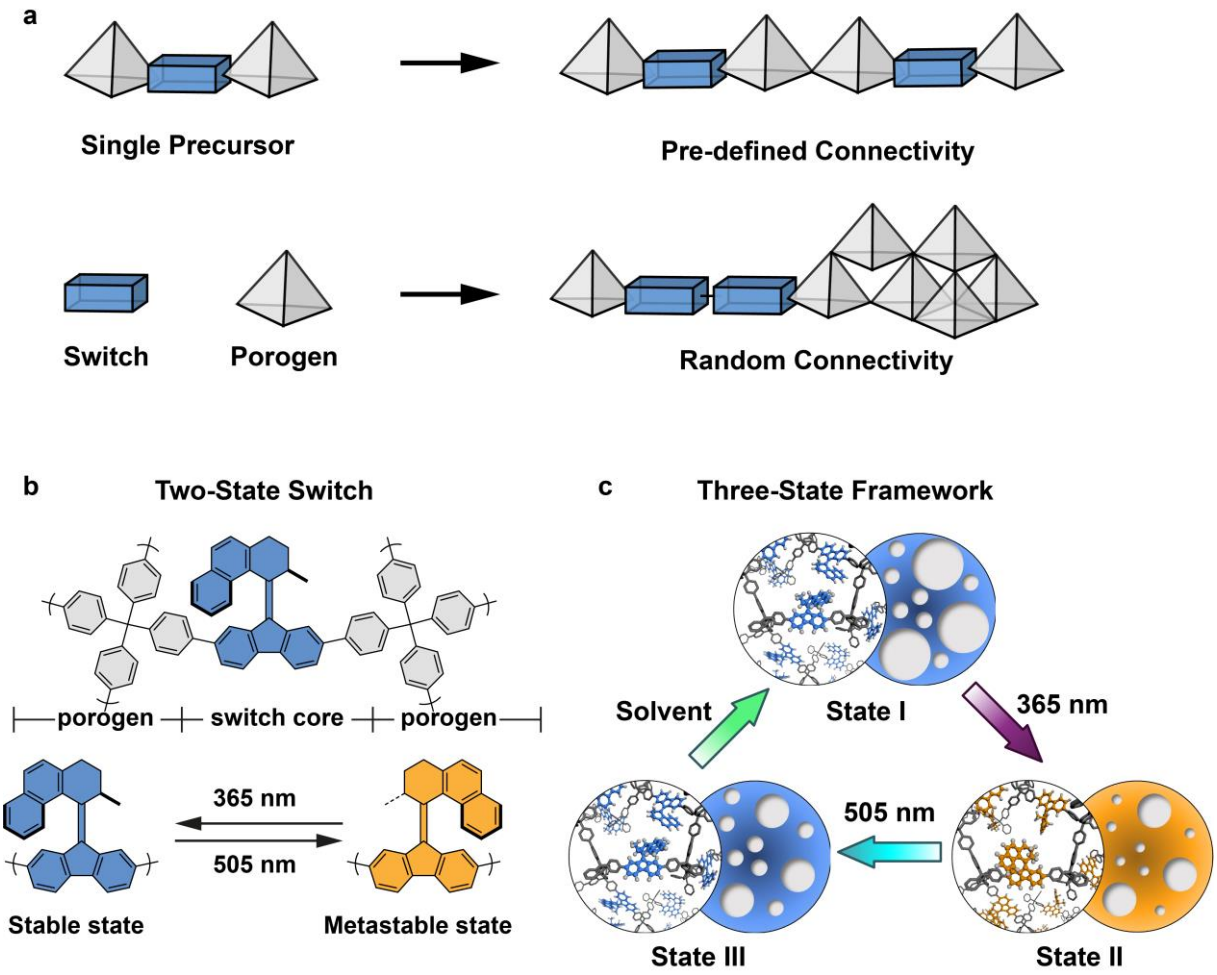

Figure 1. a. Schematic representation of two approaches for the construction of responsive PAFs. **b.** Molecular design of the multi-branch bi-stable switch and photoisomerization of the overcrowded alkene core in the porous material between two states triggered by irradiation at 365 nm and 505 nm. **c.** Schematic representation of the three distinct states of the framework material controlled reversibly by light and solvent. The micro- and meso-pores in the framework can be contracted by irradiation at 365 nm. Regeneration of micropores can be achieved by irradiation 505 nm light irradiation and of mesopores by solvent-assisted regeneration of the mesopores in the framework to the initial state.

Results and discussion

A hexabrominated monomer **1** featuring an overcrowded alkene core (Fig. 2a) was designed as a precursor with well-defined topology and containing one switch moiety between two porogenic lateral units, both to generate a highly porous homogenous aromatic framework and achieve a high concentration of photoswitch in the resulting 3D polymer. In contrast to overcrowded alkene-derived molecular motors, monomers **1** and **2** feature an expanded 6-memberd ring upper-part which pushes the naphthyl moiety closer to the fluorene stator thereby increasing the steric interactions in the molecule to the point of practical suppression of the unidirectional rotation and thermal isomerization. Consequently, **1** and **2** operate as P-type bi-stable photoswitches, reversibly switching between stable and metastable diastereomers, with the latter being stable for several years at ambient temperatures, thereby constituting ideal candidates for construction of light-addressable materials. Here, we envisioned that the highly branched architecture would allow homocoupling of the monomers into the porous aromatic framework

without the need of additional porogenic units which in turn would maximize the performance of the material upon light-induced isomerization of the responsive alkenes. In contrast to statistical co-polymerization of different monomers (Fig. 1a bottom), homo-coupling of a single precursor (Fig. 1a top) ensures the desired and pre-designed connectivity yielding a framework with a precise topology and therefore a specific property. The overcrowded alkene core **S3** was prepared (Fig 2a) by an improved Barton-Kellogg olefination,[60] which enabled large-scale synthesis (1.3 g, 3 mmol) with excellent yield (90% yield, see SI for details). The key for the improved synthesis was the utilization of electron-donating methoxy substituents in the 2,7-position of the fluorenone **S2** which rendered the thioketone **S2'** much more stable in comparison to the dibrominated analogue **S8'** and facilitated scale-up of the olefination in high yield. Subsequently, the designed-building block **1** was prepared in four additional steps involving deprotection and a series of consecutive palladium-catalysed reactions (See SI for details and characterization of new compounds) with excellent yields.

Finally, overcrowded alkene-containing monomer **1** was polymerized into the homogenous porous switchable framework (**PSF^{100}**) with controlled connectivity and topology using a Yamamoto homocoupling reaction (Fig. 2b), and the solid material was dried and activated at 85 °C under a dynamic vacuum prior to further characterization. In addition, two co-monomeric PSF materials were synthesized by hetero-coupling reaction of tetrakis(4-bromophenyl)methane (**TPM-Br$_4$**) and **1** in two different ratios (≈10% and 20% mole fraction of **1**) to yield **PSF^{10}** and **PSF^{20}** respectively to verify the impact of the switch loading on the porosity and the magnitude of the light-induced changes in porosity (Fig. 2b, synthetic details and activation procedures are reported in ESI). Furthermore, frameworks containing tribrominated overcrowded alkene **2** (Fig 2a) incorporated in the backbone of the framework denoted as porous aromatic framework-overcrowded alkene (≈10% and 20% mole fraction of **2** PAF-OA^{10} and PAF-OA^{20}, respectively) were prepared as controls to access for the difference in dynamics between backbone and pendant incorporation of the photoswitch (Fig. 2c).

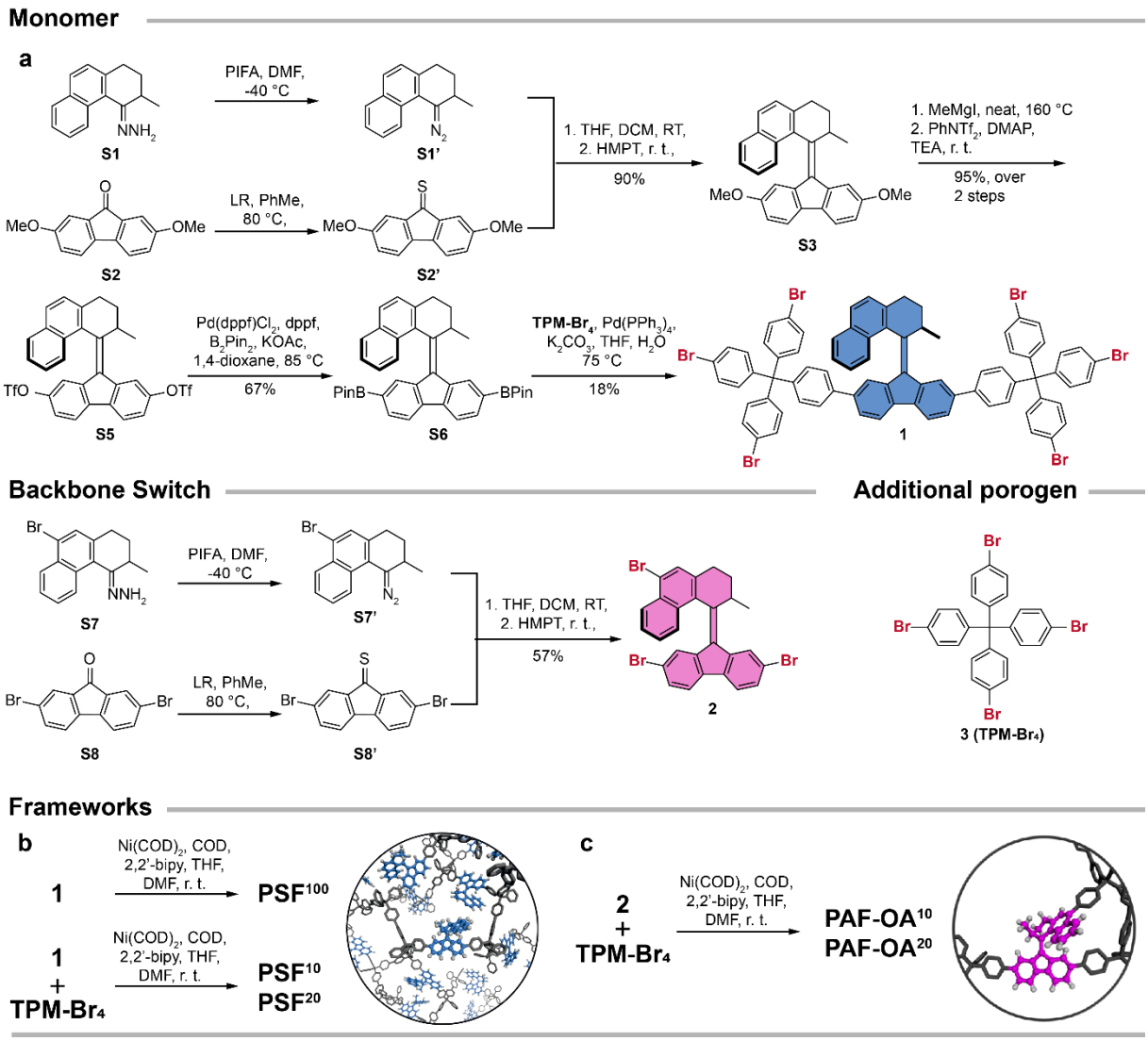

Figure 2. a. Synthesis of the multi-branch bi-stable switches **1** and **2** and structure of **TPM-Br$_4$**. **b.** and **c.** Synthesis of porous switchable frameworks (**PSFs**) by Yamamoto homo- and hetero-coupling reactions.

The remarkable porous homogeneous framework **PSF^{100}** exhibits Langmuir and Brunauer-Emmett-Teller (BET) surface areas as high as 1679 and 1482 $m^2 g^{-1}$, respectively, and a large specific total pore volume of 1.88 $cm^3 g^{-1}$, as determined by the N_2 sorption isotherms at 77 K (Fig. 3a). The **PSF^{100}** framework reveals a bimodal pore size distribution as calculated by Non-Local Density Functional Theory (NLDFT), comprising both micro- and meso-porosity that highlights a hierarchical architecture (Fig. 3b), further supported by *t-plot* analysis (Supplementary Table 7, SI section 16). The large hysteresis that closes only at low partial pressures indicates a sponge-like behaviour, in which the architecture may swell due to favourable interactions with the adsorbate and increase the mesopore capacity. Indeed, exposure of the activated **PSF^{20}** to THF led to substantial expansion of the material (40% relative linear expansion in the glass tube), indicating high flexibility of the material. (Supplementary Fig. 4). Noteworthy N_2 sorption isotherms collected at 77 K with prolonged equilibration times (up to 20 s, Supplementary Fig. 3) revealed the same hysteretic loops, indicating that the phenomenon is not associated to kinetic effects but to the mesoporosity of the framework. Similarly,

large adsorption-desorption hysteresis loops have been observed in swellable PAF-type materials.[42,61] Elemental analysis indicated nearly complete removal of the bromine atoms from the sample, which is typical for the PAF-type materials fabricated by Yamamoto cross-coupling reaction owning to the acidic work-up of the product (see Supplementary Table 3).[42,62] Nevertheless, the geometrical constraints imposed by the bent photoswitch core likely prevent a quantitative conversion of the bromides to the cross-coupled product. Instead, defects are formed by proton-termination of triphenylmethane moieties which may account for the observed large mesoporosity of the material.[61] Somewhat larger surface areas were produced under the same conditions by co-condensation of **1** with **TPM-Br$_4$** monomer: **PSF^{10}** and **PSF^{20}** (Supplementary Fig. 6) display BET surface areas as high as 2260 and 2040 $m^2\ g^{-1}$ and pore volumes of 2.10 and 2.15 $cm^3\ g^{-1}$ indicating that increasing the monomer **1** fraction does not dramatically reduce the framework porosity (Supplementary Fig. 1 and 2). Noteworthy, the similar shape of N_2 adsorption isotherms at 77 K along the expected variations in the BET surface areas for all the synthesized PSFs indicate the fabrication procedure yields materials with predictable and reproducible properties. Considering that the naphthyl moieties of the switch are expected to occupy a substantial part of the potential free volume, our successful fabrication strategy of highly porous and densely functionalized frameworks, encompassing monomers designed to form precisely defined branched networks, represents a major advance in the field of light-responsive porous materials. ^{13}C CP MAS pointed out the connectivity of monomer units and the purity of the samples, proving the effective insertion of the desired molecular species (Fig. 3c and Supplementary Fig. 5, 6). The stability of the **PSF^{100}** material was verified by thermogravimetric analysis (TGA) which indicated high thermal stability with no decomposition over 500 °C (Supplementary Fig. 7). Powder X-ray diffraction (PXRD) showed the amorphous nature of the frameworks (Supplementary Fig. 8), as expected for a material constructed by an irreversible reaction. While Yamamoto reaction may lead to a certain amount of short-range order and rigidity in pure PAFs (see Figure S5), the substantial lack of internal order in our materials induces a beneficial degree of swellability and flexibility to the framework, as testified by the large hysteresis loop, and promotes a large response upon switch isomerization. The scanning electron (SEM), and transmission electron (TEM) microscopies revealed that the **PSF** materials are comprised of small spherical nanoparticles of about 20-30 nm (Fig. 3d, 3e, and Supplementary Fig. 9-10).

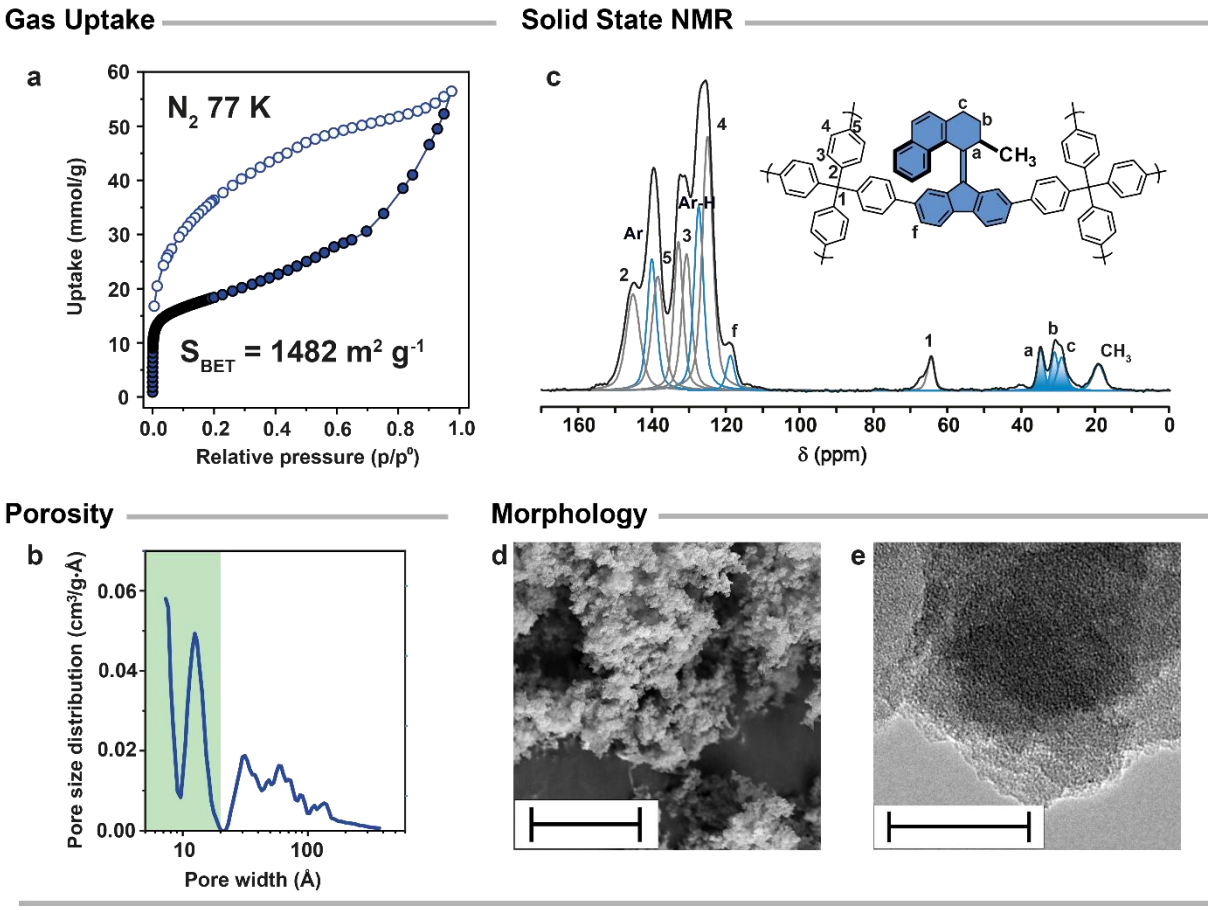

Figure 3. a. Nitrogen adsorption isotherm of **PSF^{100}** collected at 77 K. Surface areas as high as 1679 m^2/g and 1482 m^2/g were calculated according to Langmuir and BET models, respectively. **b.** Pore size distribution calculated according to NLDFT theory and carbon slit pore model. The micropore region (pore size below 20 Å) is highlighted in light green. **c.** $^{13}C\{^1H\}$ CP MAS solid state NMR of **PSF^{100}** collected with a contact time of 2 ms and magic angle spinning of 12.5 kHz. The spectrum was simulated by Lorentzian line-shape functions. **d.** SEM image of **PSF^{100}** nanoparticles (scale bar = 5 µm). **e.** TEM image of **PSF^{100}** nanoparticles (scale bar = 50 nm).

Photochemical isomerization of the monomer

Monomer **1** undergoes a photochemical isomerization upon irradiation at 365 nm from the stable to metastable diastereomer and reverts to the stable diastereomer upon irradiation at 455 nm (Fig. 4a). The switching core geometries for both the stable and metastable structures were optimized by DFT on B3LYP/6-31+G(d,p) level of theory. The double bond twisting angles are 170° and 27.5° for the stable and metastable isomers, respectively, while flipping angles (1 2 3 4) about the naphthalene plane are -51.1° and 37.5° for the stable and metastable forms, respectively, which is an 88° *flip* of carbon 4 around the naphthalene plane. This flip can be seen in the overlay of the two phases using the naphthalene moiety as a reference (Fig. 4a, Supplementary Fig. 36). Photochemical isomerization of monomer **1** in solution was followed by ^1H and ^{13}C NMR, UV/Vis electronic absorption, Raman, and IR spectroscopies (Fig. 4b-4e, Supplementary Fig. 12-13). Irradiation of a dilute solution of $\mathbf{1}_{st}$ in DCM at 365 nm led to a gradual bathochromic shift of the UV/Vis electronic absorption spectrum (Fig. 4c), which is characteristic of the photochemical formation of the metastable diastereomer $\mathbf{1}_{mst}$ via formal *E*/*Z*

isomerization of the central alkene with a quantitative yield (Fig. 4c, orange line). Subsequent irradiation at 455 nm resulted in partial reversion of $\mathbf{1_{mst}}$ to the stable diastereomer (Fig. 4c, light blue line). Throughout both processes, isosbestic points were maintained at 385 nm, confirming a clean and unimolecular isomerization. Accordingly, characteristic shifts of ^{1}H and ^{13}C NMR resonances were observed in the NMR spectra of **1** in CD_2Cl_2 upon successive irradiation at 365 nm followed by irradiation at 455 nm, which allowed to unambiguously identify and assign the respective diastereomers.[63] The composition of the photostationary state (PSS) established upon irradiation at both wavelengths was calculated by integration of aliphatic resonances in ^{1}H NMR spectrum. (Fig. 4b). Upon irradiation at 365 nm, a virtually complete photoconversion to the metastable diastereomer (7 : 93 of stable : metastable) was reached at the photostationary state (PSS_{365}). In contrast, the selectivity for the reverse process was found to be modest, and at the photostationary state (PSS_{455}), a lower photoconversion (58 : 42 of stable : metastable) to the stable diastereomer was observed (Supplementary Fig. 12). In addition, the isomerization process of **1** in solution could be conveniently followed by vibrational (Raman, IR) spectroscopies (Fig. 4e and Supplementary Fig. 14). Raman spectra revealed a distinctive difference in the spectra of both diastereomers in the region characteristic of central alkene stretching (1530 - 1590 cm^{-1}) which were previously[30] demonstrated to be diagnostic for isomerization between folded stable and twisted metastable diastereomers. Similar marked changes were observed in the FT-IR spectra between 1600 to 1500 cm^{-1}, accompanied by prominent changes in the IR spectral region characteristic of the aliphatic C-H stretching (3000 - 2800 cm^{-1}), likely originating from the conformational change of the six-membered ring associated with the isomerization (Supplementary Fig. 14). The photoisomerization process was further studied using DFT (see Supplementary Information for details) by evaluating the ground state (S_0) and the relevant excited states. The S_0 pathway shows a 32.9 kcal/mol barrier from $\mathbf{1_{st}}$ to $\mathbf{1_{mst}}$, and the latter is 5.1 kcal/mol higher than $\mathbf{1_{st}}$, which supports thermal back-switching of the metastable to the stable diastereomer (Fig. 4f-g). The TD-DFT simulated UV/Vis spectra of the photoswitch core capture qualitatively the main features of the experimental UV/Vis spectra (Fig. 4c and Supplementary Fig. 37 - 38). The simulated spectra show that only the S_1 and S_2 excited states (S_1 - HOMO → LUMO and S_2 - HOMO-1 → LUMO, Supplementary Fig. 37) exist at wavelengths longer than 365 nm (energy excitation used) for both stable and metastable diastereomers, indicating that these two excited states can participate in the photoconversion mechanism. Irradiation at 365 nm promotes the forward conversion entering the S_1 and S_2 excited states; since the S_1 pathway favours back conversion, the formation of the metastable state can only occur via the S_2 pathway (PSS_{365}=7:93 of stable : metastable, Supplementary Fig. 38-39). Under irradiation at 455 nm, the S_1 (mst) pathway is selectively excited, promoting the metastable-to-stable conversion (PSS_{455}=58:42 of stable : metastable).

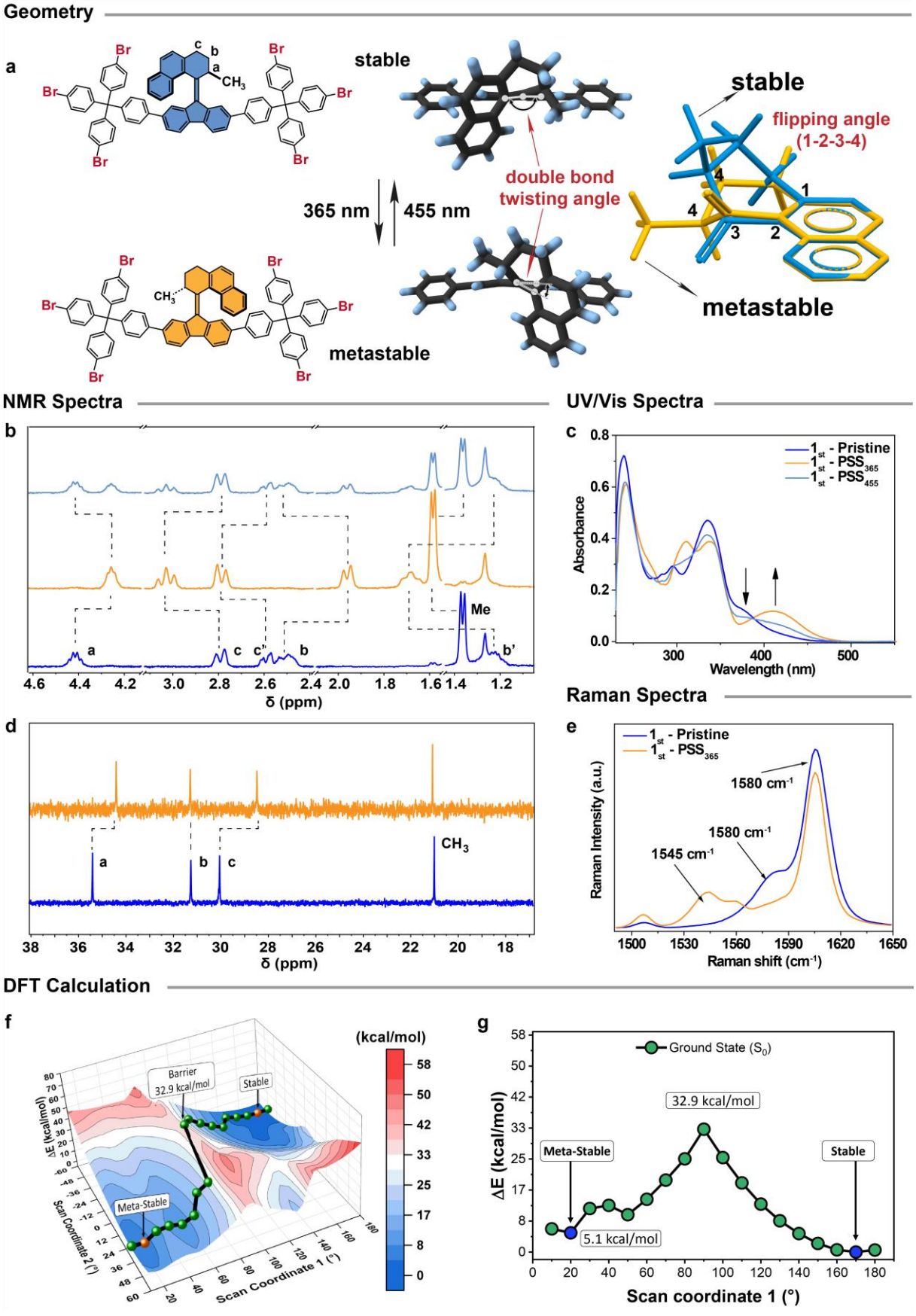

Figure 4. a. Schematic representation of the structural changes upon photoisomerization of the bistable switch **1** (**1**$_{st}$↔**1**$_{mst}$) (left panel) and DFT optimized geometries of the switching core calculated using B3LYP/6-31+G(d,p)

level of theory of both diastereomers (right panel). **b.** Comparison of the aliphatic part of the ^{1}H NMR (CD_2Cl_2, 400 MHz, RT) spectra of $\mathbf{1}_{st}$ (blue spectrum) upon irradiation at 365 nm (orange spectrum) and concomitant irradiation at 455 nm (light blue, see panel **a** for the assignment of the resonances). **c.** Changes in the UV/Vis electronic absorption spectra (DCM, 20 μM) of $\mathbf{1}_{st}$ (blue spectrum, $\mathbf{1}_{st}$-pristine) upon irradiation at 365 nm (orange spectrum, $\mathbf{1}_{st}$-PSS_{365}) and subsequent irradiation at 455 nm (light blue, $\mathbf{1}_{st}$-PSS_{455}). **d.** The comparison of the aliphatic part of the ^{13}C NMR spectra (CD_2Cl_2, 400 MHz, RT) of the $\mathbf{1}_{st}$ (blue spectra) and $\mathbf{1}_{mst}$ (spectrum of the photostationary state obtained upon irradiation at 365 nm, orange spectra). **e.** Comparison of the Raman spectra (785 nm laser) of $\mathbf{1}_{st}$ (blue spectrum, $\mathbf{1}_{st}$-pristine) and $\mathbf{1}_{mst}$ (orange spectrum, $\mathbf{1}_{mst}$-PSS_{365}). Spectra were obtained by drop-casting pristine and irradiated solutions (DCM) onto a quartz substrate. (**f**) 2D PES scan shown as a surface plot. Blue indicates low energy and red indicates high energy. The minimum energy pathway between the stable and metastable forms is overlaid using green spheres and the stable and metastable positions are indicated with orange spheres. The scale bar ranges from 0 – 58 kcal/mol. (**g**) The energy plot for the minimum energy pathway between the stable and metastable forms, twisting the double bond from 180°(stable) to 10° (meta-stable). The blue circles indicate the minima for the stable and meta-stable forms. The scan coordinates are shown in Fig. S35.

Photo-isomerization in the solid state. The photoisomerization behaviour of the frameworks comprising bistable switch **1** was investigated with UV/Vis diffuse-reflectance (DR UV/Vis), Raman, diffuse-reflectance infrared Fourier transform (DRIFT) spectroscopies and ^{13}C SS NMR (Solid State NMR) (Fig. 5b-5d and Supplementary Fig. 21). Characteristic spectral changes were observed upon irradiation of the framework $\mathbf{PSF}^{\mathbf{100}}$ (for $\mathbf{PSF}^{\mathbf{10}}$ and $\mathbf{PSF}^{\mathbf{20}}$ see Supplementary Fig. 16, 19, and 22-23) that, by comparison to the solution data, allowed us to unambiguously ascribe the main features due to photoswitching of monomer **1** in the solid state. In the DR UV/vis spectra of $\mathbf{PSF}^{\mathbf{100}}$, a large bathochromic shift was observed upon irradiation of the material at 365 nm, consistent with the reversible $\mathbf{1}_{st} \rightarrow \mathbf{1}_{mst}$ isomerization (Fig. 5b). Additionally, a new band centred at 1540 cm^{-1} was observed in the Raman spectra of the UV-irradiated $\mathbf{PSF}^{\mathbf{100}}$ material, consistent with the formation of the $\mathbf{1}_{mst}$ diastereomer (Fig. 5c). ^{13}C SS NMR spectra recorded for the irradiated material revealed upfield shifts of the aliphatic ^{13}C resonances (C_a 35.0 ppm → 34.5 ppm and C_c 29.3 ppm → 28.5 ppm), in agreement with the corresponding upfield shifts observed in solution NMR of monomer, unequivocally demonstrating photoisomerization of the overcrowded alkene embedded in the framework (Fig. 5d and Supplementary Table 4).

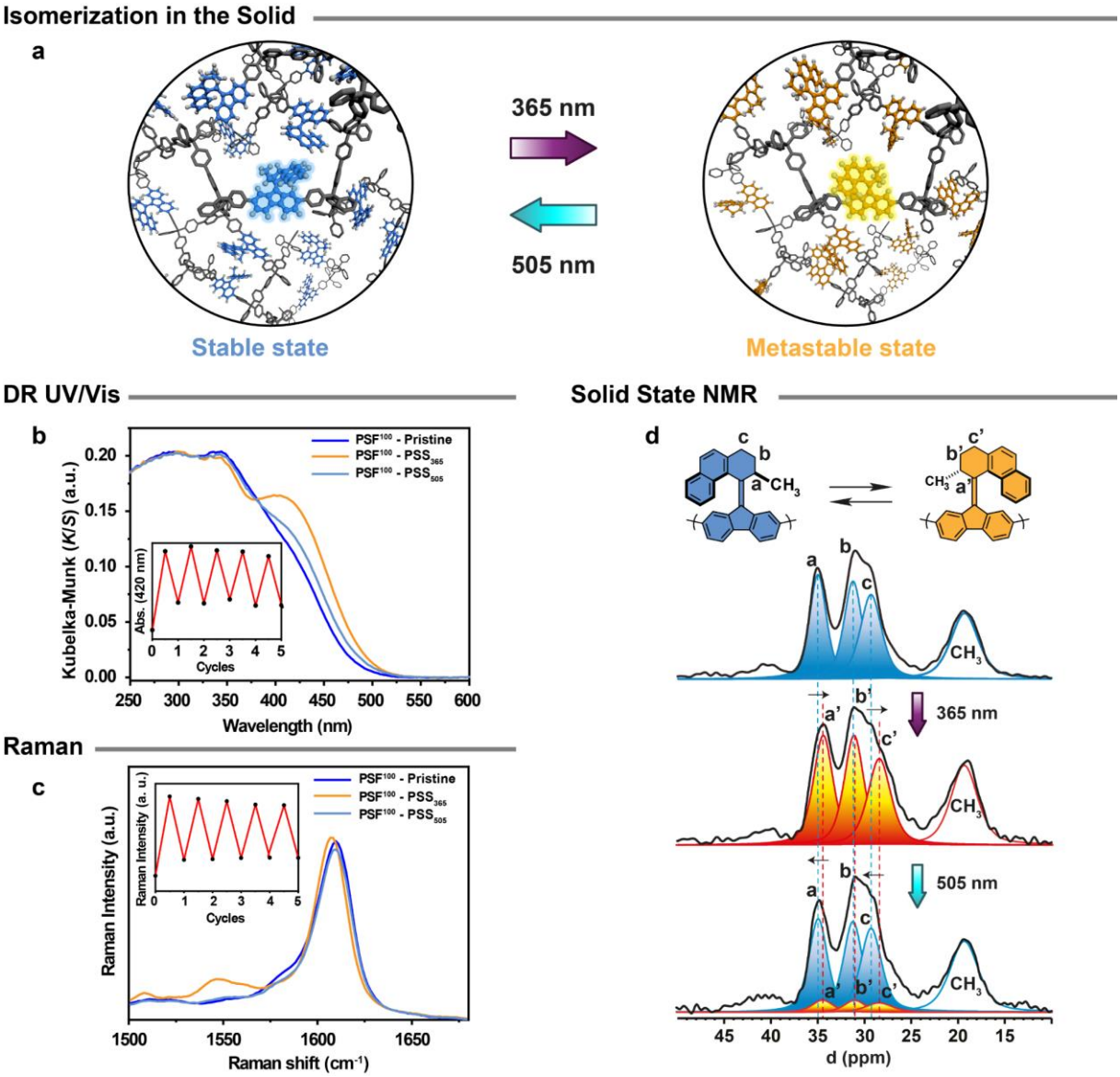

Figure 5. **a.** Schematic representation of the photoisomerization of the **PSF^{100}** materials. **b.** Changes in the Kubelka-Munk transformed DR UV/Vis spectra of the **PSF^{100}** material (blue spectra, **PSF^{100}-Pristine**) upon irradiation at 365 nm to the photostationary state (orange spectra, **PSF^{100}-PSS$_{365}$**) and subsequent irradiation at 505 nm to regenerate the stable diastereomer (light blue spectra, **PSF^{100}-PSS$_{505}$**). The inset shows changes in the Kubelka-Munk function at 420 nm upon multiple isomerization cycles. **c.** Comparison of the baselined Raman (785 nm) spectra of the **PSF^{100}** material (blue spectra, **PSF^{100}-Pristine**) upon irradiation at 365 nm to the photostationary state (orange spectra, **PSF^{100}-PSS$_{365}$**) and subsequent irradiation at 505 nm to recover the stable diastereomer (light blue spectra, **PSF^{100}-PSS$_{505}$**). The inset shows changes in the Raman intensity at 1550 cm^{-1} upon multiple isomerization cycles. **d.** $^{13}C\{^{1}H\}$ CP MAS solid state NMR of a pristine **PSF^{100}** material (top panel), after irradiation at 365 nm (middle panel) and after subsequent irradiation at 505 nm (bottom panel). See the isomerization scheme for the assignment of the ^{13}C resonances. Simulated blue and orange Lorentzian functions represent resonances characteristic of stable and metastable diastereomers, respectively.

Notably, upon extensive irradiation of **PSF^{100}** at 365 nm, complete photoconversion to the metastable diastereomer could be achieved as demonstrated by deconvolution of the quantitative ^{13}C SS NMR spectra of the bulk solid (within the accuracy of the method, Fig. 5d). Similar to the monomeric **1$_{mst}$** dissolved in solution, the back-switching of the framework could be achieved upon irradiation of the material at 455 nm with the same moderate photoconversion to the stable diastereomer as in the solution

(Supplementary Fig. 15 and 18). However, we observed that a significantly higher selectivity of the back-switching photoisomerization could be achieved using a longer wavelength, i.e. 505 nm as indicated by comparison of Raman and DR UV/Vis (Fig. 5b-5c, Supplementary Fig. 15, and 18) spectra. Indeed, quantitative analysis of the ^{13}C SS NMR spectra recorded for the **PSF^{100}**, irradiated at 505 nm, revealed a photostationary state consisting of 87% of the stable isomer: this demonstrates a much higher degree of photoconversion of the alkene in the framework compared to that achievable in solution (Fig. 5d). This solid-state behaviour is likely originating from the bathochromic shift of the bands, compared to the monomer **1$_{mst}$** in solution, in the electronic absorption spectra of the photoswitch. The red-shifted spectrum of **PSF^{100}** tails beyond 500 nm and therefore provides better spectral separation between the two diastereomers in the framework. Notably, extended (30 min) irradiation of **1$_{mst}$** at 505 nm in solution led to almost no photoconversion to **1$_{st}$** diastereomer, indicating that this phenomenon is exclusively associated with the solid state. Additional control experiments on **PSF^{10}** and **PSF^{20}** frameworks revealed similar green-light responsivity for the back-switching reaction, showing no dilution-dependence of this phenomenon in the system and that the photochemical behaviour of the photoswitch originates from unique interactions within the aromatic framework rather than from intermolecular interactions between the photoswitches (Supplementary Fig. 16). The photostability studies, performed by alternating irradiation at 365/505 nm light irradiation by Raman and DR UV/Vis spectroscopies, show negligible fatigue (note the incomplete back-isomerization in the first cycles), demonstrating the reversibility and robustness of the light-responsive material (Fig. 5b-5c insets). Further alternating irradiations at 365/505 nm followed by DR UV/Vis spectroscopy revealed a reduction of efficiency after 15 switching cycles (Supplementary Fig. 40), although, the photodamage is likely confined to the surface leaving the particle bulk substantially unaffected as no significant signs of fatigue in the SS NMR spectra (Figure 5d) of extensively irradiated **PSF^{100}**. In contrast, in the case of **PAF-OA^{20}** material (see Fig. 2c for structures) surface sensitive techniques including Raman and DR UV/Vis spectroscopies (Supplementary Fig. 17, 20, and 24-25) showed only minor changes after irradiation at 365 nm, while the solid state ^{13}C MAS NMR indicated no changes between the spectra of pristine sample and material irradiated at 365 nm, thus excluding any bulk photoisomerization of the switch (Supplementary Fig. 26). The significant constraints imposed on the photoswitches by the surrounding framework is likely restricting the photoisomerization in the bulk of the material, consequently resulting in only minor isomerization on the surface of the particles.[37]

The framework materials (**PSF^{100}**, **PSF^{20}** and **PSF^{10}**) were subject to gas sorption experiments after irradiation at 365 nm in the solid state (Fig. 6a-6e, Supplementary Fig. 27, and Table 5). Compared to the porosity of the pristine **PSF^{100}** material (state I), nitrogen adsorption isotherms of UV-irradiated **PSF^{100}** sample collected at 77 K showed lower uptake at any partial pressure: the contraction of the accessible pore volume was evidenced in both micro and mesopore regions (state II, 10% and 16%, respectively), as estimated from pore volume calculation according to NLDFT theory (Fig. 6a-6b and

Supplementary Table 5) ~~and *t-plot* analysis (Supplementary Table 7 and SI section 16).~~ The reversal of the phenomenon, corresponding only to the expansion of micropores (state III), was obtained by irradiation at 505 nm, showing recovery of 95% microporosity and full reversibility of the on/off switch cycle (Fig. 6a-6b, light blue). Notably, photoisomerization drives not only the configurational rearrangement of the bi-stable switch moiety but also a reversible reorganization of the micropore free-volume, likely due to the memory of the local molecular arrangement of the pristine material.[64] This indicates the relevance of constraints to ensure that the switch conformational tension is transmitted to the local environment of the framework and expands the micropores. Conversely, in the mesopore region manifested at higher gas loading, the porosity is not entirely recovered upon irradiation at 505 nm and the photoswitching back does not bring an efficient full recovery action because a larger conformational transmissibility through the framework is required (Fig. 6d, light blue). The complete reversion to the original state of **PSF^{100}** (state I) was successfully achieved using a chemical stimulus, i.e. by soaking in organic solvents (THF/DMF). The porous material swelled and, after drying, reacquired its maximum absorption capacity (Fig. 6c, green), exhibiting a memory effect by a solvent-assisted regeneration process. Accordingly, **PSF^{10}** and **PSF^{20}**, with a lower content of photoswitch, show a comparable lower reduction in the pore volume upon isomerization of the photoswitches, (Fig. 6e, Supplementary Fig. 28-30, and Table 5). In fact, by a systematic variation of the content of the two building blocks we can widely tune the connectivity of PSFs and consequently their gas adsorption properties. These results further indicate the direct relationship between the nanoscale photo-induced photoswitch rearrangement and the bulk contraction of the framework, proving that the insertion of the large number of the photoswitching moieties constitutes an effective strategy to modulate adsorption properties (Supplementary Table 5).

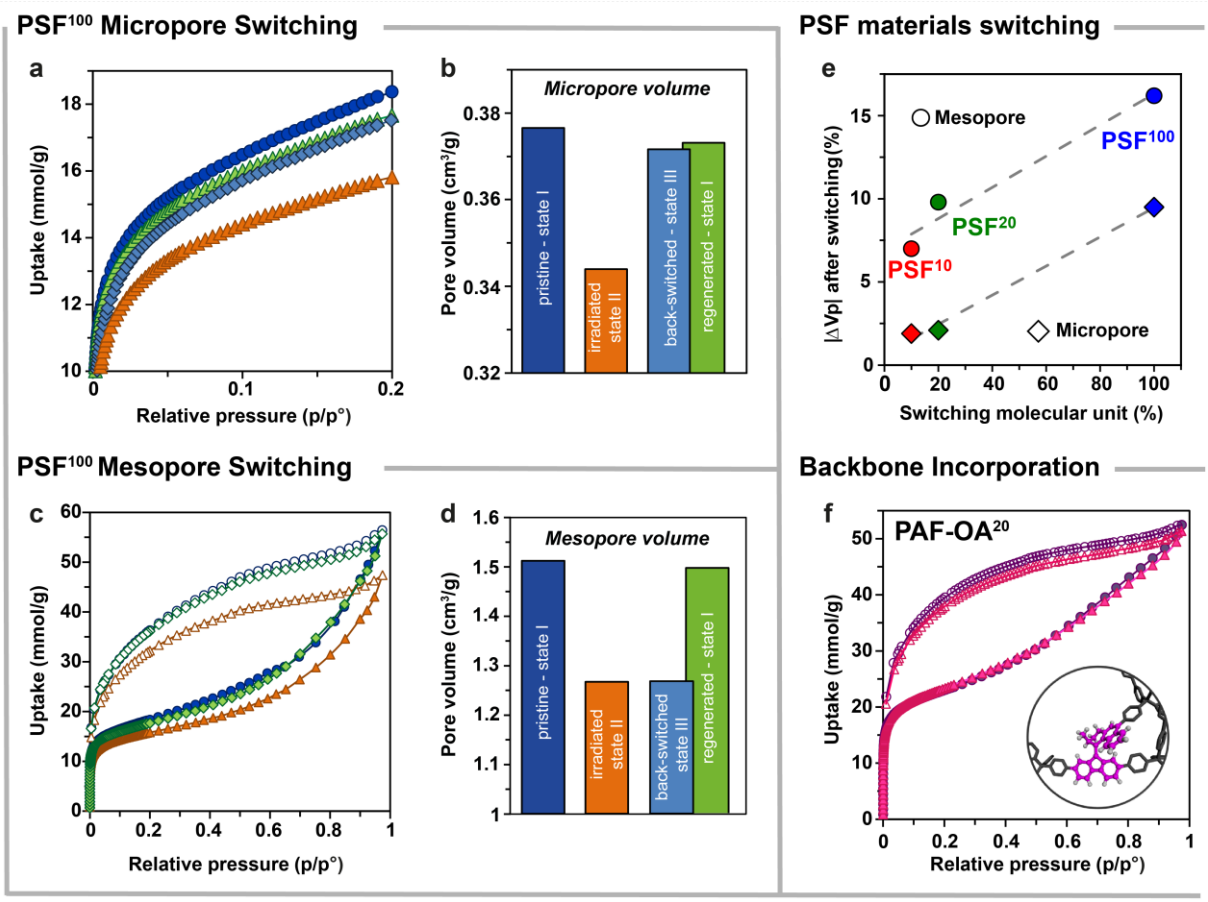

Figure 6. a. N_2 adsorption isotherms collected at 77 K and up to 0.2 p/p° of pristine **PSF^{100}** (state I, dark blue circles), after irradiation at 365 nm (state II, orange triangles), after back optical switch by irradiation at 505 nm (state III, light blue diamonds) and solvent-assisted regeneration of **PSF^{100}** (state I, green triangles), showing the modulation of nitrogen uptake at low partial pressures. **b.** Modulation of micropore volume related to pores with a diameter below 20 Å for **PSF^{100}** during the irradiation cycle and solvent-assisted regeneration process. **c.** N_2 adsorption isotherms collected between 0 and 1 p/p° at 77 K for pristine **PSF^{100}** (dark blue circles), after irradiation at 365 nm (orange triangles) and solvent-assisted regeneration of **PSF^{100}** (green triangles). **d.** Calculated mesopore volume of **PSF^{100}** over irradiation cycle and solvent-assisted regeneration process (mesoporosity between 2 and 50 nm). **e.** Decrease of the micropore and mesopore volumes of samples PSF^{10}, PSF^{20}, and PSF^{100} after UV irradiation (365 nm). The absolute change in pore volume correlates with the increased amount of photoswitches in the frameworks. **f.** N_2 adsorption isotherms collected at 77 K of pristine **PAF-OA^{20}** (dark purple) and after irradiation at 365 nm (pink). Inset: sketch of the framework with the bistable switch highlighting its three-fold connectivity.

Importantly, in the case of a non-responsive **PAF-OA^{20}** framework, significant changes in N_2 adsorption isotherms were not observed between pristine and irradiated samples (Fig. 6f), strongly supporting that the observed modulation in the gas adsorption capacity of **PSF^{100}** originates exclusively from the photoisomerization of the bistable switch. In particular, this observation, along with the activation method of the material (see Supplementary Information of synthetic section) rules out heating of the material upon irradiation as the source of the observed performance differences, since the light-induced heat generation should be maximized in the case of a non-responsive chromophore.[58] Overall, these results highlight the paramount importance of the proper interplay of conformational freedom in a responsive network necessary to enable hierarchical amplification from the stimuli-controlled nanoscale motion to the control of the breathing of the structure. This material displays outstanding surface area

and pore volume among all other photoresponsive porous materials (Supplementary Table 6) and reversible bulk photoswitching behaviour in the solid state, setting a benchmark for the design of photocontrolled porous solids.

Conclusion

The design-by-purpose hexa-branched molecular-switch monomer allowed for a novel polymerization strategy, which generates a 3D poly-switch porous framework, wherein each monomer unit has an intrinsic photoswitching element. We demonstrated that the interplay of the dynamic elements, that is the bi-stable photoswitch and flexible backbone, systematically alternated in a robust covalent architecture realized three vastly distinct states of porosity in the framework that could be accessed in sequence upon exposure to external stimuli to produce a complete duty cycle. The large pore volume combined with a hierarchical pore structure of the photoactive material allowed full optical control over micropore contraction/expansion cycles. Consistently, contraction of the mesopores was commanded by optical stimuli, while full recovery to the permanent mesoporosity was assisted by solvent-swelling, regenerating the pristine material. The densely interconnected covalent network generates unique solid-state interactions which promoted unprecedented enhancement in the wavelength selectivity of bulk photochemical isomerization in the porous solid relative to the same switch in solution.

Control experiments demonstrated the relationship between the switch content and the extent of the modulation of the adsorptive properties of PSFs and highlighted the subtle interplay between the optimal degree of freedom of photoswitches and framework responsivity. Owing to the irreversible nature of the reaction, deviations from the procedure are expected to yield the materials with distinct properties. Therefore, this approach is versatile and may generate a large family of materials, leading to frameworks with tailor-made properties for selected application. These findings will facilitate the application of these materials in on-command reconfigurable gas adsorption or separation systems. In particular, the interplay of large hysteresis between adsorption and desorption branches and light-controlled size of the micropores in our material offers opportunities for the fabrication of on-demand switchable membranes for size-selective separation operating at high working capacities. In addition, further efforts dedicated to the fabrication of optically pure frameworks based on these inherent helical switches will provide opportunities to explore chiroptical switching in solid materials. In a broader context, our work illustrates that the design and synthesis of proper monomers integrating the light-responsive elements provides opportunities for the fabrication of flexible porous frameworks exhibiting new properties or states emerging from the cooperativity and intimacy between molecular functions. Future efforts aimed at engineering the intricate combination of the rigidity and flexibility of the responsive-frameworks will allow to harness and amplify the molecular-scale motion of the light-driven artificial molecular machines more effectively and ultimately convert it into plethora of practical outputs, similar to the operating principle of nanoscopic biological machines.[4]

References

1. Goulet-Hanssens, A., Eisenreich, F., & Hech, S. Enlightening Materials with Photoswitches. Adv.Mater., **32**, 1905966 (2020).

2. Kitagawa, S. & Uemura, K. Dynamic porous properties of coordination polymers inspired by hydrogen bonds. *Chem. Soc. Rev.* **34**, 109–119 (2005).

3. He, A. *et al.* A smart and responsive crystalline porous organic cage membrane with switchable pore apertures for graded molecular sieving. *Nat. Mater.* **21**, 463–470 (2022).

4. Krause, S. & Feringa, B. L. Towards artificial molecular factories from framework-embedded molecular machines. *Nat. Rev. Chem.* **4**, 550–562 (2020).

5. Feng, L., Astumian, R. D. & Stoddart, J. F. Controlling dynamics in extended molecular frameworks. *Nat. Rev. Chem.* **6**, 705–725 (2022).

6. Vukotic, V. N., Harris, K. J., Zhu, K., Schurko, R. W. & Loeb, S. J. Metal-organic frameworks with dynamic interlocked components. *Nat. Chem.* **4**, 456–460 (2012).

7. Zhu, K., O'Keefe, C. A., Vukotic, V. N., Schurko, R. W. & Loeb, S. J. A molecular shuttle that operates inside a metal-organic framework. *Nat. Chem.* **7**, 514–519 (2015).

8. Comotti, A., Bracco, S. & Sozzani, P. Molecular Rotors Built in Porous Materials. *Acc. Chem. Res.* **49**, 1701–1710 (2016).

9. Bracco, S. *et al.* CO_2 regulates molecular rotor dynamics in porous materials. *Chem. Commun.* **53**, 7776–7779 (2017).

10. Bracco, S. *et al.* Ultrafast Molecular Rotors and Their CO_2 Tuning in MOFs with Rod-Like Ligands. *Chem. Eur. J.* **23**, 11210–11215 (2017).

11. Shivanna, M., Yang, Q. Y., Bajpai, A., Patyk-Kazmierczak, E. & Zaworotko, M. J. A dynamic and multi-responsive porous flexible metal–organic material. *Nat. Commun.* **9**, 1–7 (2018).

12. Perego, J. *et al.* Fast motion of molecular rotors in metal–organic framework struts at very low temperatures. *Nat. Chem.* **12**, 845–851 (2020).

13. Perego, J. *et al.* Cascade Dynamics of Multiple Molecular Rotors in a MOF: Benchmark Mobility at a Few Kelvins and Dynamics Control by CO_2. *J. Am. Chem. Soc.* **143**, 13082–13090 (2021).

14. Comotti, A., Bracco, S., Ben, T., Qiu, S. & Sozzani, P. Molecular rotors in porous organic frameworks. *Angew. Chem. Int. Ed.* **53**, 1043–1047 (2014).

15. Vogelsberg, C. S. *et al.* Dynamics of Molecular Rotors Confined in Two Dimensions: Transition from a 2D Rotational Glass to a 2D Rotational Fluid in a Periodic Mesoporous Organosilica. *J. Phys. Chem. B* **116**, 1623–1632 (2012).

16. Pérez-Estrada, S., Rodríguez-Molina, B., Maverick, E. F., Khan, S. I. & Garcia-Garibay, M. A. Throwing in a Monkey Wrench to Test and Determine Geared Motion in the Dynamics of a Crystalline One-Dimensional (1D) Columnar Rotor Array. *J. Am. Chem. Soc.* **141**, 2413–2420 (2019).

17. Lee, J. *et al.* Metal-organic framework materials as catalysts. *Chem. Soc. Rev.* **38**, 1450–1459 (2009).

18. Kreno, L. E. *et al.* Metal-organic framework materials as chemical sensors. *Chem. Rev.* **112**, 1105–1125 (2012).

19. Slater, A. G. & Cooper, A. I. Function-led design of new porous materials. *Science.* **348**, aaa8075 (2015).

20. Hanikel, N., Prévot, M. S. & Yaghi, O. M. MOF water harvesters. *Nat. Nanotechnol.* **15**, 348–355 (2020).

21. Feringa, B. L.and Browne, W. R. Eds., *Molecular Switches*, Wiley-VCH Verlag GmbH & Co. KGaA, Weinheim, Germany, 2011. doi:10.1002/9783527634408.

22. Zbigniew L. Pianowski. Eds.,*Molecular Photoswitches*. Wiley-VCH Verlag GmbH & Co. KGaA, Weinheim, Germany, 2022. doi:10.1002/9783527827626.

23. Browne, W. R. & Feringa, B. L. Making molecular machines work. *Nat. Nanotechnol.* **1**, 25–35 (2006).

24. Balzani, V., Credi, A. & Venturi, M. Light powered molecular machines. *Chem. Soc. Rev.* **38**, 1542–1550 (2009).

25. Erbas-Cakmak, S., Leigh, D. A., McTernan, C. T. & Nussbaumer, A. L. Artificial Molecular Machines. *Chem. Rev.* **115**, 10081–10206 (2015).

26. Costil, R., Holzheimer, M., Crespi, S., Simeth, N. A. & Feringa, B. L. Directing Coupled Motion with Light: A Key Step Toward Machine-Like Function. *Chem. Rev.* **121**, 13213–13237 (2021).

27. Coskun, A., Banaszak, M., Astumian, R. D., Stoddart, J. F. & Grzybowski, B. A. Great expectations: can artificial molecular machines deliver on their promise? *Chem. Soc. Rev.* **41**, 19–30 (2012).

28. Aprahamian, I. The Future of Molecular Machines. *ACS Cent. Sci.* **6**, 347–358 (2020).

29. Danowski, W., Van Leeuwen, T., Browne, W. R. & Feringa, B. L. Photoresponsive porous materials. *Nanoscale Adv.* **3**, 24–40 (2021).

30. Castiglioni, F. *et al.* Modulation of porosity in a solid material enabled by bulk photoisomerization of an overcrowded alkene. *Nat. Chem.* **12**, 595–602 (2020).

31. Chen, Q. *et al.* A Redox-Active Bistable Molecular Switch Mounted inside a Metal-Organic Framework. *J. Am. Chem. Soc.* **138**, 14242–14245 (2016).

32. Danowski, W. *et al.* Unidirectional rotary motion in a metal–organic framework. *Nat. Nanotechnol.* **14**, 488–494 (2019).

33. Coudert, F. X. Responsive metal-organic frameworks and framework materials: Under pressure, taking the heat, in the spotlight, with friends. *Chem. Mater.* **27**, 1905–1916 (2015).

34. Castellanos, S., Kapteijn, F. & Gascon, J. Photoswitchable metal organic frameworks: Turn on the lights and close the windows. *CrystEngComm* **18**, 4006–4012 (2016).

35. Furukawa, H., Cordova, K. E., O'Keeffe, M. & Yaghi, O. M. The chemistry and applications of metal-organic frameworks. *Science.* **341**, 1230444 (2013).

36. Zhou, H. C. J. & Kitagawa, S. Metal-Organic Frameworks (MOFs). *Chem. Soc. Rev.* **43**, 5415–5418 (2014).

37. Krause, S. *et al.* Cooperative light-induced breathing of soft porous crystals via azobenzene buckling. *Nat. Commun.* **13**, (2022).

38. Diercks, C. S. & Yaghi, O. M. The atom, the molecule, and the covalent organic framework. *Science.* **355**, eaal1585 (2017).

39. Feng, X., Ding, X. & Jiang, D. Covalent organic frameworks. *Chem. Soc. Rev.* **41**, 6010–6022 (2012).

40. Das, G. *et al.* Azobenzene-Equipped Covalent Organic Framework: Light-Operated Reservoir. *J. Am. Chem. Soc.* **141**, 19078–19087 (2019).

41. Stähler, C. *et al.* Light-driven molecular motors embedded in covalent organic frameworks. *Chem. Sci.* **13**, 8253–8264 (2022).

42. Tian, Y. & Zhu, G. Porous Aromatic Frameworks (PAFs). *Chem. Rev.* **120**, 8934–8986 (2020).

43. Zhu, Y. & Zhang, W. Reversible tuning of pore size and CO2 adsorption in azobenzene functionalized porous organic polymers. *Chem. Sci.* **5**, 4957–4961 (2014).

44. Brown, J. W. *et al.* Photophysical pore control in an azobenzene-containing metal-organic framework. *Chem. Sci.* **4**, 2858–2864 (2013).

45. Kundu, P. K., Olsen, G. L., Kiss, V. & Klajn, R. Nanoporous frameworks exhibiting multiple stimuli responsiveness. *Nat. Commun.* **5**, 1–9 (2014).

46. Lyndon, R. *et al.* Dynamic photo-switching in metal-organic frameworks as a route to low-energy carbon dioxide capture and release. *Angew. Chem. Int. Ed.* **52**, 3695–3698 (2013).

47. Park, J. *et al.* Reversible alteration of CO_2 adsorption upon photochemical or thermal treatment in a metal-organic framework. *J. Am. Chem. Soc.* **134**, 99–102 (2012).

48. Nikolayenko, V. I., Herbert, S. A. & Barbour, L. J. Reversible structural switching of a metal-organic framework by photoirradiation. *Chem. Commun.* **53**, 11142–11145 (2017).

49. Fan, C. Bin *et al.* Significant Enhancement of C_2H_2/C_2H_4 Separation by a Photochromic Diarylethene Unit: A Temperature- and Light-Responsive Separation Switch. *Angew. Chemie - Int. Ed.* **56**, 7900–7906 (2017).

50. Luo, F. *et al.* Photoswitching CO_2 capture and release in a photochromic diarylethene metal-organic framework. *Angew. Chem. Int. Ed.* **53**, 9298–9301 (2014).

51. Zheng, Y. *et al.* Flexible interlocked porous frameworks allow quantitative photoisomerization in a crystalline solid. *Nat. Commun.* **8**, 1–6 (2017).

52. Williams, D. E. *et al.* Energy transfer on demand: Photoswitch-directed behavior of metal-porphyrin frameworks. *J. Am. Chem. Soc.* **136**, 11886–11889 (2014).

53. Furlong, B. J. & Katz, M. J. Bistable Dithienylethene-Based Metal-Organic Framework Illustrating Optically Induced Changes in Chemical Separations. *J. Am. Chem. Soc.* **139**, 13280–13283 (2017).

54. Williams, D. E. *et al.* Flipping the Switch: Fast Photoisomerization in a Confined Environment. *J. Am. Chem. Soc.* **140**, 7611–7622 (2018).

55. Dolgopolova, E. A. *et al.* Connecting Wires: Photoinduced Electronic Structure Modulation in Metal-Organic Frameworks. *J. Am. Chem. Soc.* **141**, 5350–5358 (2019).

56. Baroncini, M. *et al.* Photoinduced reversible switching of porosity in molecular crystals based on star-shaped azobenzene tetramers. *Nat. Chem.* **7**, 634–640 (2015).

57. Wang, Z. *et al.* Series of Photoswitchable Azobenzene-Containing Metal-Organic Frameworks with Variable Adsorption Switching Effect. *J. Phys. Chem. C* **122**, 19044–19050 (2018).

58. Castellanos, S. *et al.* Structural Effects in Visible-Light-Responsive Metal-Organic Frameworks Incorporating ortho-Fluoroazobenzenes. *Chem. Eur. J.* **22**, 746–752 (2016).

59. Wang, Z. *et al.* Tunable molecular separation by nanoporous membranes. *Nat. Commun.* **7**, 1–7 (2016).

60. Pooler, D. R. S., Lubbe, A. S., Crespi, S. & Feringa, B. L. Designing light-driven rotary molecular motors. *Chem. Sci.* **12**, 14964–14986 (2021).

61. Perego, J., Piga, D., Bracco, S., Sozzani, P. & Comotti, A. Expandable porous organic

frameworks with built-in amino and hydroxyl functions for CO_2 and CH_4 capture. *Chem. Commun.* **54**, 9321–9324 (2018).

62. Ben, T. *et al.* Targeted Synthesis of a Porous Aromatic Framework with High Stability and Exceptionally High Surface Area. *Angew. Chem. Int. Ed.* **48**, 9457–9460 (2009).

63. Sheng, J. *et al.*Designing P-type bi-stable overcrowded alkene-based chiroptical photoswitches. *Chem. Sci.* doi.org/10.1039/D2SC05903G.

64. Rozyyev, V. *et al.* High-capacity methane storage in flexible alkane-linked porous aromatic network polymers. *Nat. Energy* **4**, 604–611 (2019).

Acknowledgements

This work was supported from the following sources: China Scholarship Council (CSC PhD Fellowship No. 201808330459 to J.S., No. 201707040079 to X.Z.), China Postdoctoral Science Foundation (grant No. 2021M691003 to S.Y.C). We acknowledge the generous financial support from the Horizon 2020 Framework Program (ERC Advanced Investigator Grant No. 694345 to BLF), and the Ministry of Education, Culture and Science of the Netherlands (Gravitation Program No. 024.001.035 to BLF). The Ministero dell'Istruzione, dell'Università e della Ricerca for MIUR-Progetto Dipartimenti di Eccellenza 2018-2022, PRIN 20173L7W8K (NEMO), PRIN (SHERPA) and Lombardy Region for "Enhancing Photosynthesis" grant (2021-2023) are acknowledged for the financial support. R. Sneep is acknowledged for mass spectral analysis. We thank Qi Zhang from university of Groningen for fruitful discussions and Piotr Cieciórski from University of Warsaw for the design of Fig. 1.

Author contributions

J.S., W.D. and B.L.F. conceived the project. B.L.F. and A.C. guided and supervised the research. J.S. synthesized the building blocks and all materials. J.S. carried out the UV and NMR irradiation studies in solution. X.Z. and J.S. carried out the SEM and TEM measurements. J.S. performed elemental analysis, DR-UV-vis and FT-IR measurements. S.C. and W.D. conducted Raman measurements. J.P. performed thermogravimetric analysis, solid state irradiation, gas adsorption isotherms. S.K. supported sample activation and adsorption analysis. S.B. carried solid state irradiation and solid state NMR spectra. C.X.B. performed computational studies. J.S., W.D., J.P., A.C., S.B., P.S. and B.L.F. wrote the manuscript. All authors discussed the results and commented on the manuscript.